7 Deep Inelastic Scattering

Verlockend ist der äußre Schein
der Weise dringet tiefer ein.

Wilhelm Busch
Der Geburtstag

7.1 Excited States of the Nucleons

In Sect. 5.5 we discussed the spectra observed in electron scattering off nuclei. As well as the elastic scattering peak some additional peaks, which we associated with nuclear excitations, were observed. Similar spectra are observed for electron-nucleon scattering.

Figure 7.1 shows a spectrum from electron-proton scattering. It was obtained at an electron energy $E = 4.9$ GeV and at a scattering angle of $\theta = 10°$ by varying the accepted scattering energy of a magnetic spectrometer in small steps. Besides the sharp elastic scattering peak (scaled down by a factor of 15 for clarity) peaks at lower scattering energies are observed associated with inelastic excitations of the proton. These peaks correspond to excited states of the nucleon, which we call *nucleon resonances*. The existence of these excited states of the proton demonstrates that the proton is a composite system. In Chap. 15 we will explain the structure of these resonances in the framework of the quark model.

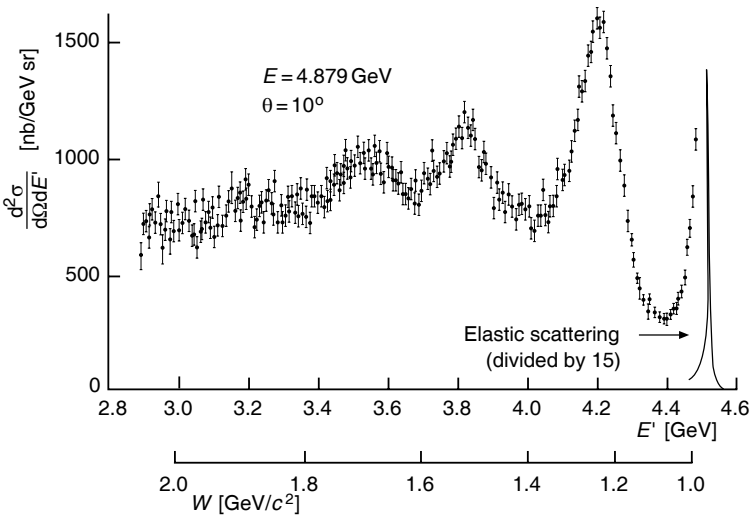

Fig. 7.1. Spectrum of scattered electrons from electron–proton scattering at an electron energy of $E = 4.9$ GeV and a scattering angle of $\theta = 10°$ (from [Ba68]).

The invariant mass of these states is denoted by W. It is calculated from the four-momenta of the exchanged photon (q) and of the incoming proton (P) according to

$$W^2c^2 = P'^2 = (P+q)^2 = M^2c^2 + 2Pq + q^2 = M^2c^2 + 2M\nu - Q^2 \,. \quad (7.1)$$

Here the Lorentz-invariant quantity ν is defined by

$$\nu = \frac{Pq}{M} \,. \quad (7.2)$$

The target proton is at rest in the laboratory system, which corresponds to $P = (Mc, \mathbf{0})$ and $q = ((E - E')/c, \boldsymbol{q})$. Therefore the energy transferred by the virtual photon from the electron to the proton in the laboratory frame is:

$$\nu = E - E' \,. \quad (7.3)$$

The Δ(1232) resonance. The nucleon resonance $\Delta(1232)$, which appears in Fig. 7.1 at about $E' = 4.2$ GeV, has a mass $W = 1232\,\mathrm{MeV}/c^2$. As we will see in Chap. 15, this resonance exists in four different charge states: Δ^{++}, Δ^{+}, Δ^{0}, and Δ^{-}. In Fig. 7.1, the Δ^{+} excitation is observed since charge is not transferred in the reaction.

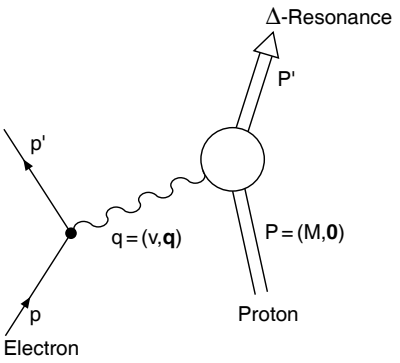

The width observed for the elastic peak is a result of the finite resolution of the spectrometer, but resonances have a real width[1] of typically $\Gamma \approx 100\,\mathrm{MeV}$. The uncertainty principle then implies that such resonances have very short lifetimes. The $\Delta(1232)$ resonance has a width of approximately 120 MeV and thus a lifetime of

$$\tau = \frac{\hbar}{\Gamma} = \frac{6.6 \cdot 10^{-22}\,\mathrm{MeV\,s}}{120\,\mathrm{MeV}} = 5.5 \cdot 10^{-24}\,\mathrm{s} \,. \quad (7.4)$$

This is the typical time scale for strong interaction processes. The Δ^{+} resonance decays by:

$$\Delta^{+} \to \mathrm{p} + \pi^{0}$$
$$\Delta^{+} \to \mathrm{n} + \pi^{+} \,.$$

A light particle, the π-meson (or pion) is produced in such decays in addition to the nucleon.

[1] The exact meaning of "width" will be discussed in Sect. 9.2.

7.2 Structure Functions

Individual resonances cannot be distinguished in the excitation spectrum for invariant masses $W \gtrsim 2.5\ \mathrm{GeV}/c^2$. Instead, one observes that many further strongly interacting particles (hadrons) are produced.

The dynamics of such production processes may be, similarly to the case of elastic scattering, described in terms of form factors. In the inelastic case they are known as the W_1 and W_2 structure functions.

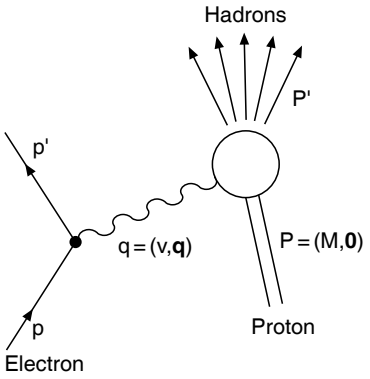

In *elastic* scattering, at a given beam energy E, there is only *one* free parameter. For example, if the scattering angle θ is fixed, kinematics requires that the squared four-momentum transfer Q^2, the energy transfer ν, the energy of the scattered electron E' etc. are also fixed. Since $W = M$, (7.1) yields the relationship:

$$2M\nu - Q^2 = 0\ . \tag{7.5}$$

In *inelastic* scattering, however, the excitation energy of the proton adds a further degree of freedom. Hence these structure functions and cross-sections are functions of *two* independent, free parameters, e. g., (E', θ) or (Q^2, ν). Since $W > M$ in this case, we obtain

$$2M\nu - Q^2 > 0\ . \tag{7.6}$$

The Rosenbluth formula (6.10) is now replaced by the cross-section:

$$\frac{\mathrm{d}^2\sigma}{\mathrm{d}\Omega\,\mathrm{d}E'} = \left(\frac{\mathrm{d}\sigma}{\mathrm{d}\Omega}\right)^*_{\mathrm{Mott}} \left[W_2(Q^2,\nu) + 2W_1(Q^2,\nu)\tan^2\frac{\theta}{2}\right]\ . \tag{7.7}$$

The second term again contains the magnetic interaction.

The first *deep inelastic* scattering experiments were carried out in the late sixties at SLAC, using a linear electron accelerator with a maximum energy of 25 GeV. Figure 7.2 shows spectra of scattering off hydrogen obtained at a fixed scattering angle $\theta = 4°$. In the graphs, $\mathrm{d}^2\sigma/\mathrm{d}\Omega\,\mathrm{d}E'$ is plotted as a function of W at several fixed beam energies E between 4.5 GeV and 20 GeV. Each spectrum covers a different range of Q^2 from $0.06 < Q^2 < 0.09\ (\mathrm{GeV}/c)^2$ to $1.45 < Q^2 < 1.84\ (\mathrm{GeV}/c)^2$. It can be clearly seen that the cross-sections drop off rapidly with Q^2 in the range of the nucleon resonances. For increasing W, however, the falloff is less pronounced.

The behaviour above the resonance region was, however, surprising. Here, the counting rates were much larger than was expected in view of the results

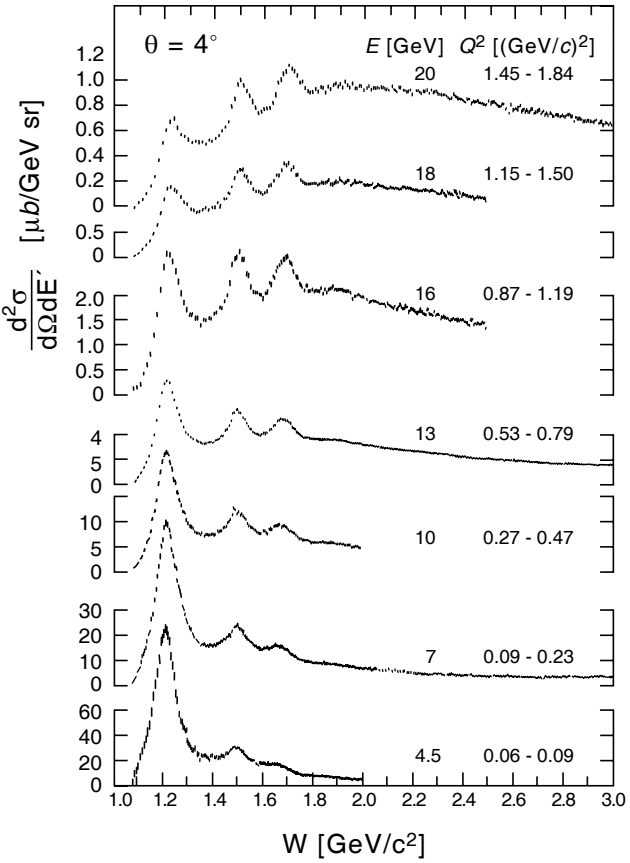

Fig. 7.2. Electron-proton scattering: excitation spectra measured in deep inelastic electron–nucleon scattering as functions of the invariant mass W [St75]. Note the different scales of the y-axis. The measurements were taken at a fixed scattering angle, $\theta = 4^\circ$. The average Q^2-range of the data increases with increasing beam energy E. The resonances, in particular the first one ($W = 1.232$ GeV/c^2), become less and less pronounced, but the continuum ($W \gtrsim 2.5$ GeV/c^2) decreases only slightly.

from elastic scattering, or from the excitation of the Δ resonance. Figure 7.3 shows the ratio:

$$\frac{\mathrm{d}^2\sigma}{\mathrm{d}\Omega\,\mathrm{d}E'} \Bigg/ \left(\frac{\mathrm{d}\sigma}{\mathrm{d}\Omega}\right)^*_{\mathrm{Mott}} \tag{7.8}$$

measured in these experiments as a function of Q^2 at different values of W. It can be seen that this ratio only depends weakly on Q^2 for $W > 2$ GeV/c^2, in clear contrast to the rapid drop with $|G^{\,\mathrm{dipole}}|^2 \approx 1/Q^8$ for elastic scattering

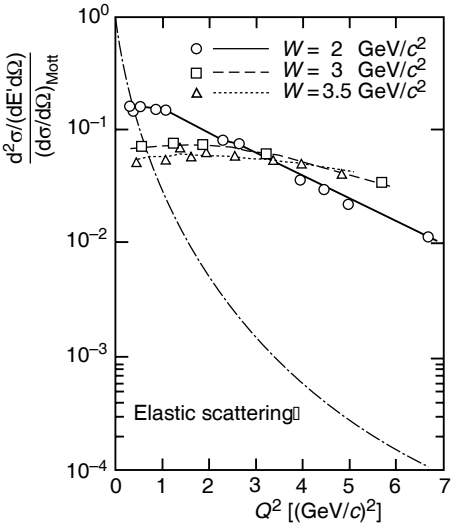

Fig. 7.3. Electron–proton scattering: measured cross-sections normalised to the Mott cross-sections as functions of Q^2 at different values of the invariant mass W [Br69].

(6.12). Hence, in deep inelastic scattering, the structure functions W_1 and W_2 are nearly independent of Q^2 for fixed values of the invariant mass W.

To better discuss this result, we introduce a new Lorentz-invariant quantity, the *Bjorken scaling variable*.

$$x := \frac{Q^2}{2Pq} = \frac{Q^2}{2M\nu} \,. \tag{7.9}$$

This dimensionless quantity is a measure of the inelasticity of the process. For elastic scattering, in which $W = M$, (7.5) yields:

$$2M\nu - Q^2 = 0 \quad \Longrightarrow \quad x = 1 \,. \tag{7.10}$$

However, for inelastic processes, in which $W > M$, we have:

$$2M\nu - Q^2 > 0 \quad \Longrightarrow \quad 0 < x < 1 \,. \tag{7.11}$$

The two dimensionful structure functions $W_1(Q^2, \nu)$ and $W_2(Q^2, \nu)$ are usually replaced by two dimensionless structure functions:

$$\begin{aligned} F_1(x, Q^2) &= Mc^2\, W_1(Q^2, \nu) \\ F_2(x, Q^2) &= \nu\, W_2(Q^2, \nu) \,. \end{aligned} \tag{7.12}$$

If one extracts $F_1(x, Q^2)$ and $F_2(x, Q^2)$ from the cross-sections, one observes at fixed values of x that they depend only weakly, or not at all, on Q^2. This

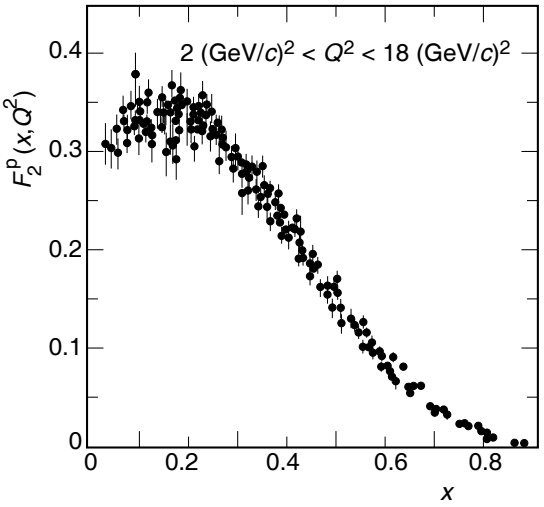

Fig. 7.4. The structure function F_2 of the proton as a function of x, for Q^2 between 2 $(\mathrm{GeV}/c)^2$ and 18 $(\mathrm{GeV}/c)^2$ [At82].

is shown in Fig. 7.4 where $F_2(x, Q^2)$ is displayed as a function of x, for data covering a range of Q^2 between 2 $(\mathrm{GeV}/c)^2$ and 18 $(\mathrm{GeV}/c)^2$.

The fact that the structure functions are independent of Q^2 means, according to our previous discussion, that the electrons are scattered off a point charge (cf. Fig. 5.6). Since nucleons are extended objects, it follows from the above result that:

nucleons have a sub-structure made up of point-like constituents.

The F_1 structure function results from the magnetic interaction. It vanishes for scattering off spin zero particles. For spin 1/2 Dirac particles (6.5) and (7.7) imply the relation:

$$2xF_1(x) = F_2(x)\,. \tag{7.13}$$

This is called the *Callan-Gross relation* [Ca69] (see the exercises).

The ratio $2xF_1/F_2$ is shown in Fig. 7.5 as a function of x. It can be seen that the ratio is, within experimental error, consistent with unity. Hence we can further conclude that:

the point-like constituents of the nucleon have spin 1/2.

7.3 The Parton Model

The interpretation of deep inelastic scattering off protons may be considerably simplified if the reference frame is chosen judiciously. The physics of the

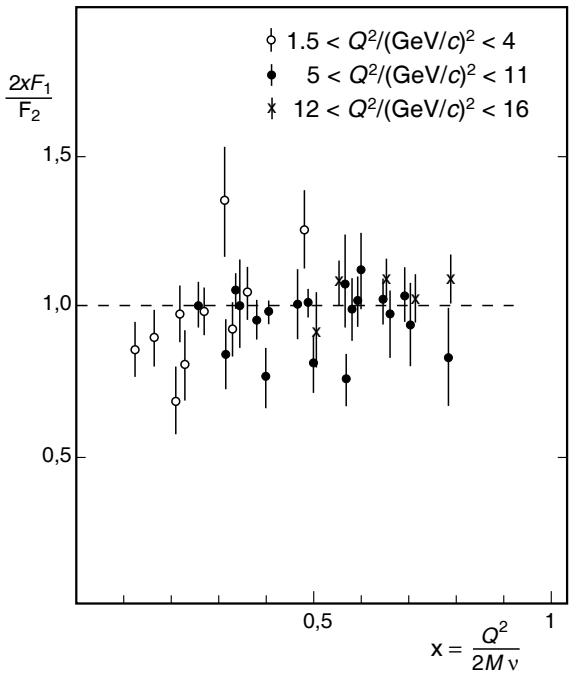

Fig. 7.5. Ratio of the structure functions $2xF_1(x)$ and $F_2(x)$. The data are from experiments at SLAC (from [Pe87]). It can be seen that the ratio is approximately constant (≈ 1).

process is, of course, independent of this choice. If one looks at the proton in a fast moving system, then the transverse momenta and the rest masses of the proton constituents can be neglected. The structure of the proton is then given to a first approximation by the longitudinal momenta of its constituents. This is the basis of the *parton model* of Feynman and Bjorken. In this model the constituents of the proton are called *partons*. Today the charged partons are identified with the quarks and the electrically neutral ones with the gluons, the field quanta of the strong interaction.

Decomposing the proton into free moving partons, the interaction of the electron with the proton can be viewed as the incoherent sum of its interactions with the individual partons. These interactions in turn can be regarded as elastic scattering. This approximation is valid as long as the duration of the photon-parton interaction is so short that the interaction between the partons themselves can be safely neglected (Fig. 7.6). This is the *impulse approximation* which we have already met in quasi-elastic scattering (p. 78). In deep inelastic scattering this approximation is valid because the interaction between partons at short distances is weak, as we will see Sect. 8.3.

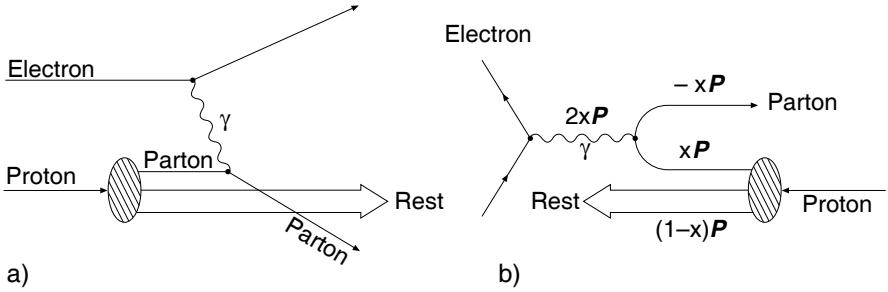

Fig. 7.6. Schematic representation of deep inelastic electron-proton scattering according to the parton model, in the laboratory system (**a**) and in a fast moving system (**b**). This diagram shows the process in two spatial dimensions. The arrows indicate the directions of the momenta. Diagram (**b**) depicts the scattering process in the Breit frame in which the momentum transferred by the virtual photon is zero. Hence the momentum of the struck parton is turned around but its magnitude is unchanged.

If we make this approximation and assuming both that the parton masses can be safely neglected and that $Q^2 \gg M^2c^2$, we obtain a direct interpretation of the Bjorken scaling variable $x = Q^2/2M\nu$, which we defined in (7.9). It is that fraction of the four-momentum of the proton which is carried by the struck parton. A photon which, in the laboratory system, has four-momentum $q=(\nu/c, \boldsymbol{q})$ interacts with a parton carrying the four-momentum xP. We emphasise that this interpretation of x is only valid in the impulse approximation, and then only if we neglect transverse momenta and the rest mass of the parton; i. e., in a very fast moving system.

A popular reference frame satisfying these conditions is the so-called *Breit frame* (Fig. 7.6b), where the photon does not transfer any energy ($q_0 = 0$). In this system x is the three-momentum fraction of the parton.

The spatial resolution of deep inelastic scattering is given by the reduced wave-length $\lambda\!\!\!^{-}$ of the virtual photon. This quantity is not Lorentz-invariant, but depends upon the reference frame. In the laboratory system ($q_0 = \nu/c$) it is:

$$\lambda\!\!\!^{-} = \frac{\hbar}{|\boldsymbol{q}|} = \frac{\hbar c}{\sqrt{\nu^2 + Q^2c^2}} \approx \frac{\hbar c}{\nu} = \frac{2Mx\hbar c}{Q^2}\,. \tag{7.14}$$

For example, if $x = 0.1$ and $Q^2 = 4\,(\mathrm{GeV}/c)^2$ one finds $\lambda\!\!\!^{-} \simeq 10^{-17}\,\mathrm{m}$ in the laboratory system. In the Breit frame, the equation simplifies to

$$\lambda\!\!\!^{-} = \frac{\hbar}{|\boldsymbol{q}|} = \frac{\hbar}{\sqrt{Q^2}}\,. \tag{7.15}$$

Q^2 therefore has an obvious interpretation in the Breit frame: it fixes the spatial resolution with which structures can be studied.

7.4 Interpretation of Structure Functions in the Parton Model

Structure functions describe the internal composition of the nucleon. We now assume the nucleon to be built from different types of quarks f carrying an electrical charge $z_f \cdot e$. The cross-section for electromagnetic scattering from a quark is proportional to the square of its charge, and hence to z_f^2.

We denote the distribution function of the quark momenta by $q_f(x)$, i. e. $q_f(x)\mathrm{d}x$ is the expectation value of the number of quarks of type f in the hadron whose momentum fraction lies within the interval $[x, x + \mathrm{d}x]$. The quarks responsible for the quantum numbers of the nucleon are called *valence quarks*. Additionally quark–antiquark pairs are found in the interior of nucleons. They are produced and annihilated as virtual particles from the gluons in the field of the strong interaction. This process is analogous to the production of virtual electron–positron pairs in the Coulomb field. These quarks and antiquarks are called *sea quarks*.

The momentum distribution of the antiquarks is denoted by $\bar{q}_f(x)$, and accordingly that of the gluons by $g(x)$. The structure function F_2 is then the sum of the momentum distributions weighted by x and z_f^2. Here the sum is over all types of quarks and antiquarks:

$$F_2(x) = x \cdot \sum_f z_f^2 \left(q_f(x) + \bar{q}_f(x)\right) \ . \tag{7.16}$$

The structure functions were determined by scattering experiments on hydrogen, deuterium and heavier nuclei. By convention in scattering off nuclei the structure function is always given per nucleon. Except for small corrections due to the Fermi motion of the nucleons in the deuteron, the structure function of the deuteron F_2^{d} is equal to the average structure function of the nucleons F_2^{N}:

$$F_2^{\mathrm{d}} \approx \frac{F_2^{\mathrm{p}} + F_2^{\mathrm{n}}}{2} =: F_2^{\mathrm{N}} \ . \tag{7.17}$$

Hence the structure function of the neutron may be determined by subtracting the structure function of the proton from that of the deuteron.

In addition to electrons, muons and neutrinos can also used as beam particles. Like electrons, muons are point-like, charged particles. There is an advantage in using them, as they can be produced with higher energies than electrons. The scattering processes are completely analogous, and the cross-sections are identical. Neutrino scattering yields complementary information about the quark distribution. Neutrinos couple to the weak charge of the quarks via the weak interaction. In neutrino scattering, it is possible to distinguish between the different types of quarks, and also between quarks and antiquarks. Details will be given in Sect. 10.8.

x-dependence of the structure functions. Combining the results of neutrino and antineutrino scattering yields the momentum distribution of the sea quarks and of the valence quarks separately. The shape of the curves in Fig. 7.7 shows that sea quarks contribute to the structure function only at small values of x. Their momentum distribution drops off rapidly with x and is negligible above $x \approx 0.35$. The distribution of the valence quarks has a maximum at about $x \approx 0.2$ and approaches zero for $x \to 1$ and $x \to 0$. The distribution is smeared out by the Fermi motion of the quarks in the nucleon.

For large x, F_2 becomes extremely small. Thus it is very unlikely that *one* quark alone carries the major part of the momentum of the nucleon.

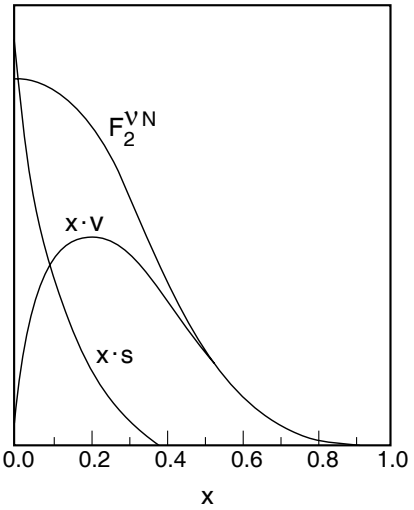

Fig. 7.7. Sketch of the structure function F_2 of the nucleon as measured in (anti)neutrino scattering. Also shown are the momentum distributions, weighted by x, of the valence quarks (v) and sea quarks (s).

Nuclear effects. Typical energies in nuclear physics (e. g., binding energies) are of the order of several MeV and typical momenta (e. g., Fermi momenta) are of the order of 250 MeV/c. These are orders of magnitude less than the Q^2 values of scattering experiments used to determine the structure functions. Therefore one would expect the structure functions to be the same for scattering off free nucleons or scattering off nucleons bound in nuclei, except, of course, for kinematic effects due to the Fermi motion of the nucleons in the nucleus. In practice, however, a definite influence of the surrounding nuclear medium on the momentum distribution of the quarks is observed [Ar94]. This phenomenon is called the *EMC Effect* after the collaboration which detected it in 1983.

For illustration, Fig. 7.8 shows the ratio of the structure functions of calcium and deuterium. The fraction of the isotope ^{40}Ca in natural calcium is 97 %. It is the heaviest stable nuclide which is an isoscalar; i. e., which has equal numbers of protons and neutrons. Deuterium, on the other hand, is

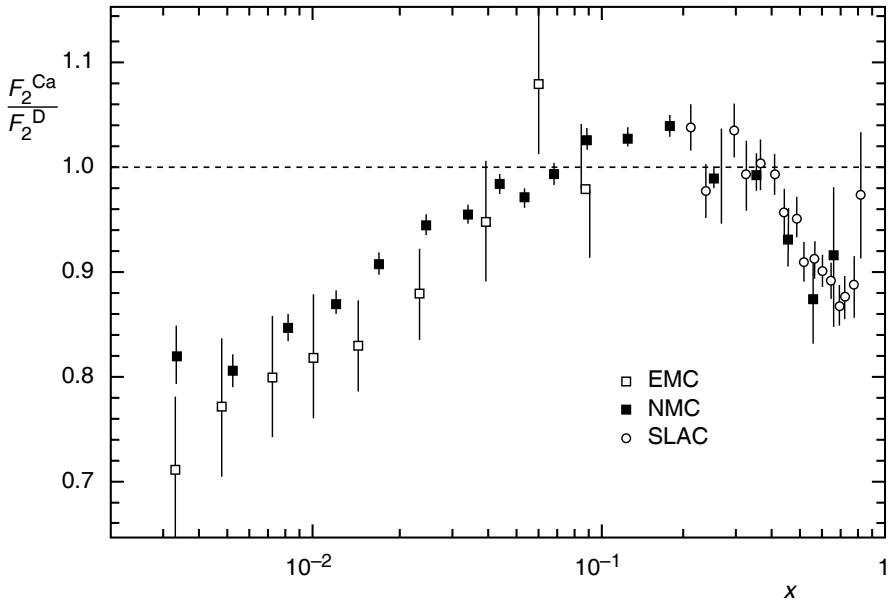

Fig. 7.8. Ratio of the structure functions F_2 of calcium and deuterium as a function of x [Ar88, Go94b, Am95].

only weakly bound, and its proton and neutron can be roughly considered to be free nucleons. The advantage of comparing isoscalar nuclides is that we can study the influence of nuclear binding on the structure function F_2, without having to worry about the differences between F_2^{p} and F_2^{n}.

A distinct deviation of the ratio from unity is visible throughout the entire x-range. For $x \lesssim 0.06$, the ratio is smaller than unity, and decreases with decreasing values of x. In this range the structure functions are dominated by the sea quarks. For $0.06 \lesssim x \lesssim 0.3$, the ratio is slightly larger than unity. In the range $0.3 \lesssim x \lesssim 0.8$ where the valence quarks prevail, the ratio is again smaller than unity, with a minimum at $x \approx 0.65$. For large values of x, it increases rapidly with x. The rapid change of the ratio in this region disguises the fact that the absolute changes in F_2 are very small since the structure functions themselves are tiny. Measurements with different nuclei show a strong increase of the EMC effect with increasing mass number A at small values of x and a weak increase in the range of intermediate values of x.

Notwithstanding the small size of the observed effects, they have generated great theoretical interest. They could contain key information for understanding the nuclear force on the basis of the fundamental interaction between quarks and gluons. We will expand upon this point in Sect. 16.3.

Theoretical models for the explanation of the EMC effect are abundant [Ar94]. So far, none of the models is able to convincingly describe the phenomena over the entire range of x. This suggests that the effect is probably due to several factors. Some possible explanations for the EMC effect are: interactions between quarks in different nucleons; the "swelling" of the radius of the nucleon within the nucleus; coalescence of nucleons to form "multiquark clusters" of 6, 9, ... valence quarks; kinematical effects caused by the reduction in the effective nucleon mass due to nuclear binding; correlation between nucleons; Fermi motion — and many other reasons.

In general, despite great theoretical effort, there is no single commonly accepted picture of the physics underlying the dependence of the structure functions on the nuclear environment.

Problems

1. **Compton scattering**
   At the HERA collider ring the spins of the electrons going around the ring align themselves over time antiparallel to the magnetic guide fields (Sokolov-Ternov effect [So64]). This spin polarisation may be measured with the help of the spin dependence of Compton scattering. We solely consider the kinematics below.
   a) Circularly polarised photons from an argon laser (514 nm) hit the electrons (26.67 GeV, straight flight path) head on. What energy does the incoming photon have in the rest frame of the electron?
   b) Consider photon scattering through 90° and 180° in the electron rest frame. What energy does the scattered photon possess in each case? How large are the energies and scattering angles in the lab frame?
   c) How good does the spatial resolution of a calorimeter have to be if it is 64 m away from the interaction vertex and should spatially distinguish between these photons?

2. **Deep inelastic scattering**
   Derive the Callan-Gross relation (7.13). Which value for the mass of the target must be used?

3. **Deep inelastic scattering**
   Deep inelastic electron-proton scattering is studied at the HERA collider. Electrons with 30 GeV are collided head on with 820 GeV protons.
   a) Calculate the centre of mass energy of this reaction. What energy does an electron beam which hits a stationary proton target have to have to reproduce this centre of mass energy?

b) The relevant kinematical quantities in deep inelastic scattering are the square of the four momentum transfer Q^2 and the Bjorken scaling variable x. Q^2 may, e.g., be found from (6.2). Only the electron's kinematical variables (the beam energy E_e, the energy of the scattered electron E'_e and the scattering angle θ) appear here. In certain kinematical regions it is better to extract Q^2 from other variables since their experimental values give Q^2 with smaller errors. Find a formula for Q^2 where the scattering angles of the electron θ and of the scattered quark γ appear. The latter may be determined experimentally from measurements of the final state hadron energies and momenta. How?

c) What is the largest possible four momentum transfer Q^2 at HERA? What Q^2 values are attainable in experiments with stationary targets and 300 GeV beam energies? What spatial resolution of the proton does this value correspond to?

d) Find the kinematical region in Q^2 and x that can be reached with the ZEUS calorimeter which covers the angular region 7° to 178°. The scattered electron needs to have at least 5 Gev energy to be resolved.

e) The electron-quark interaction can occur through neutral currents (γ, Z^0) or through charged ones ($W^{\pm}$). Estimate at which value of Q^2 the electromagnetic and weak interaction cross-sections are of the same size.

4. **Spin polarisation**
Muons are used to carry out deep inelastic scattering experiments at high beam energies. First a static target is bombarded with a proton beam. This produces charged pions which decay in flight into muons and neutrinos.

a) What is the energy range of the muons in the laboratory frame if magnetic fields are used to select a 350 GeV pion beam?

b) Why are the spins of such a monoenergetic muon beam polarised? How does the polarisation vary as a function of the muon energy?

5. **Parton momentum fractions and x**
Show that in the parton model of deep inelastic scattering, if we do **not** neglect the masses of the nucleon M and of the parton m, the momentum fraction ξ of the scattered parton in a nucleon with momentum P is given by

$$\xi = x\left[1 + \frac{m^2c^2 - M^2c^2x^2}{Q^2}\right].$$

In the deep inelastic domain $\frac{x^2M^2c^2}{Q^2} \ll 1$ and $\frac{m^2c^2}{Q^2} \ll 1$. (Hint: for small ε, ε' we can approximate $\sqrt{1+\varepsilon(1+\varepsilon')} \approx 1 + \frac{\varepsilon}{2}(1 + \varepsilon' - \frac{\varepsilon}{4})$.)